Macromolecules

pubs.acs.org/Macromolecules
Article

A Reactive Bead−Spring Model for Associative Polymer Melts In and Out of Equilibrium

Songyue Liu and Thomas C. O'Connor*

Cite This: *Macromolecules* 2024, 57, 1403−1413
Read Online
ACCESS | Metrics & More | Article Recommendations

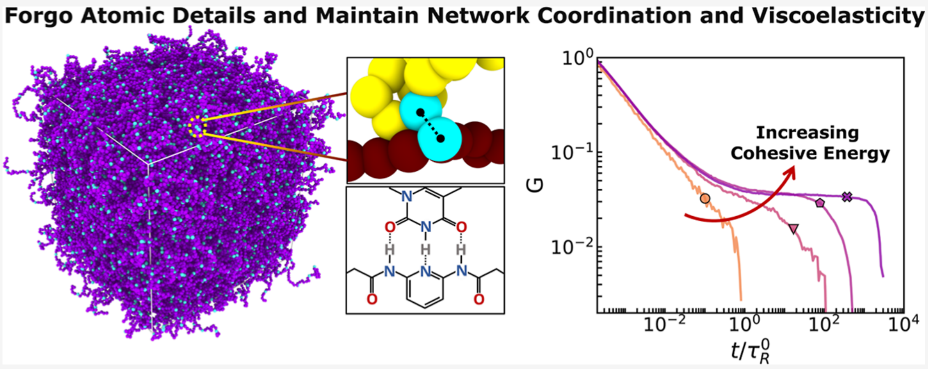

ABSTRACT: We describe a new coarse-grained reactive molecular dynamics model for associative polymer networks. Our model combines a Tersoff bond-order potential for associative bond chemistry with a standard bead−spring model for molten polymers. The resulting model captures the essential physics of chain dynamics, chain entanglement, and coordinated dynamic bonding and can be tuned to capture a variety of associative bond kinetics. The many-body Tersoff Hamiltonian for dynamic bonding remains valid in nonequilibrium flow conditions, unlike Monte Carlo methods based on equilibrium bond kinetics. We use this model to simulate polymer melts with binary associative bonds of varying cohesive strength. We measure the gelation transition with increasing association strength and identify a gel point at an associative bond strength $\sim 1k_BT$. We also assess how chain dynamics and network viscoelasticity change as the degree of gelation increases and relate them to the microscopic kinetics of dynamic bond exchange.

■ INTRODUCTION

Associating or dynamic polymer networks are topologically adaptive elastomers formed through the assembly of reconfigurable associative chemical bonds between polymer chains.[1] Nature is adept at harnessing such associative interactions to drive biopolymers to form complex and adaptive self-assembled structures.[2] Associative bonds like hydrogen bonds and $\pi-\pi$ bonds are also common in many commodity polymers such as polyamides[3] like nylon[4] and Kevlar,[5] where they dramatically alter polymer material structure, thermomechanical properties, and processing. Inspired by biopolymers in nature, many researchers are working to incorporate associative bonds into commodity polymer chains to create sustainable reprocessable polymers as replacements for unrecyclable thermosets and thermoplastic.[1,6,7] Replacing strong covalent cross-links with thermoreversible associative bonds enables the creation of robust networks that can be reprocessed at elevated temperatures.[1,6−8] However, these same fluctuations in chain connectivity produce complex chain dynamics and viscoelasticity that are hard to describe in equilibrium and largely unexplored in nonequilibrium processing conditions.[9]

Many experimental and theoretical studies have improved our molecular understanding of associative polymer networks in equilibrium. Analytic models based on mean-field scaling laws like the reversible gelation model,[10,11] sticky Rouse,[12] and sticky reptation[13,14] can accurately fit experimentally observed linear viscoelastic behavior in a wide variety of dynamic networks. They reasonably work well for equilibrium systems when the time and length scales associated with different molecular processes are well-separated—associations are well-spaced along chains—and the network structure is uniform throughout the material.[15] However, in many biological and

Received: October 4, 2023
Revised: December 15, 2023
Accepted: January 12, 2024
Published: February 5, 2024

https://doi.org/10.1021/acs.macromol.3c02022

synthetic systems of current interest, these assumptions do not hold when sticker spacing is comparable to Kuhn length or the strand is stiff.[9] Current models are proving insufficient to relate the viscoelastic properties of these networks to their underlying molecular structures.[9] Additionally, mean-field models average over the fluctuations to predict an average structure and dynamics, which fail to describe nonequilibrium systems. Fluctuations can couple with flows to produce heterogeneous dynamics and structures, giving rise to complex processing behaviors.[16]

New models are needed to capture the complex processing behavior, but the microscopic details of associative networks in nonequilibrium conditions are difficult to access in experiments. Many studies have turned to molecular simulations to relate the molecular structure of networks to their viscoelastic dynamics. Simulation studies model associative bond kinetics through hybrid molecular dynamics (MD)/Monte Carlo (MC) simulation[17−21] and pure MC[22−24] or MD methods.[25−33] However, many of these models require making prescriptive assumptions about associative kinetics and how they behave in nonequilibrium flow conditions. For example, models using MC steps to perform associative reactions require user-specified reaction rates for the association and disassociation processes. These are usually based on steady−state equilibrium reactions, and it is not always clear how these should be modified under nonequilibrium conditions. While nonequilibrium MC methods are an active area of research, rules for their use are not well-established, especially when combined with MD simulations.[17,34]

To regulate the cluster size and bond directionality of associative groups, researchers have developed MD approaches that model associative functional groups as rigid multibead clusters of particles that interact through pair potentials.[32,33,35,36] By fusing a small sticky subparticle on one side of a targeted monomer into a rigid body, these models produce reversible directional bonds with controllable coordination. The geometry and interactions of such composite particles can be varied to reproduce a wide variety of systems, including dimerizing fluids,[36] self-assembly in DNA-like and collagen-like peptides,[37−39] and phase behavior[32] and viscoelasticity of oligomer systems with hydrogen bonds.[33] Since these approaches leverage pair potentials, they tend to be computationally efficient and relatively easy to implement in existing MD codes. Their main drawback is that designing composite associative groups with desired bond energies and coordination can be challenging, requiring careful balancing of pairwise attractions and steric exclusion. This makes composite-particle strategies less ideal when one wants to systematically vary bond exchange kinetics and bond coordination.

Reactive force-fields are another popular strategy for simulating reversible bonding with MD. They employ many-body potential energies to classically approximate the physics of dynamic chemical bonding during MD simulations.[40,41] Popular reactive models like the Stillinger-Weber, Tersoff, ReaxFF, COMB, and REBO models have been applied to a wide variety of metallic, organic, and inorganic molecular and bulk material systems.[42−45] Reactive force-fields are usually applied to fully atomistic systems, providing a classical bridge between quantum-electronic physics and atomic dynamics. However, they can also be employed at coarse-grained scales to model many-body free energies that depend upon the local (coarse-grained) atomic environment. This approach has been used to create coarse-grained reactive models for water in biomolecular simulations, catalytic systems, and covalent adaptive networks.[46−48]

The major limitation of deploying reactive models is their complicated functional forms, which require fitting many parameters simultaneously. For this reason, these tools have only recently begun being applied to simulate associative interactions in coarse-grained polymer systems. Sciortino et al.[25] recently developed a minimal reactive potential to model bond-swapping dynamics by incorporating a coordination-dependent three-body potential that allows complementary stickers to dimerize and swap bonds. The rate of swapping is tuneable by adjusting the energy barrier for bond-swapping. This method has been utilized to study the dynamics of vitrimers[26−28,30] and reversible polymer gels with different architectures.[31] This minimal model is easily implemented and captures the essential physics of associative bonding, but its functional form is somewhat limited to forming binary complexes between two complementary species of sticky monomers and cannot be easily generalized to more complicated associative complexes like metal−ligand coordination.

In this paper, we present a new coarse-grained reactive model for simulating the dynamics of associative polymer networks both in equilibrium and during nonequilibrium processing flows. Our model combines a standard Kremer−Grest bead−spring model with a customized Tersoff bond order potential that captures the dynamics of associative bonds and precisely controls the coordination and kinetics of the associative complexes. This allows the new model to simulate coarse-grained representations of associative systems arising from a diversity of underlying chemical interactions, including hydrogen bonds, ionic bonds, and adaptive covalent chemistry. Unlike MC methods for dynamic bonding, which require the modeler to specify kinetic rates for bond formation and scission a priori, the bond kinetics of our model emerge naturally from the reactive potential energy landscape. This means that our model can make *predictions* about changes in associative kinetics as polymer architecture, composition, and flow are varied.

We demonstrate our model's ability to capture the self-assembly and gelation of associative networks with bond kinetics controlled by a tuneable energy barrier. We examine two models with different barriers controlling the binary bond-exchange process and relate their equilibrium viscoelasticity to changes in the underlying dynamic bond kinetics. For the degrees of gelation that we consider, we observe a simple relationship between the network terminal relaxation time and the so-called "brachiation time"—i.e., the average time for an unpaired associative site to find an associative partner. Note, while this study focuses on associations that form binary complexes, like hydrogen bonds, our reactive model can be generalized to capture higher coordinations and more complex reaction kinetics.

■ MODELS AND METHODS

Coarse-Grained Polymer Melts. Our model combines the standard Kremer−Grest bead−spring model[49] with a three-body Tersoff potential[45] that captures the "coarse-grained chemistry" of associative bonding. The Tersoff functional form can be tuned to control dynamic bond coordination, directionality, and environment-dependent bond energies.

All beads have a unitless mass $m_0 = 1.0$ and interact with a purely repulsive, truncated Lennard−Jones (LJ) potential with an LJ energy, distance, and time scale denoted by ϵ_{LJ}, σ, and $\tau_{\mathrm{LJ}} = \sqrt{(m_0\sigma^2/\epsilon_{\mathrm{LJ}})}$, respectively. All physical simulation quantities are reported in these reduced LJ units. 4000 linear chains of length $N = 40$ beads are bonded by a finitely extensible nonlinear elastic potential.[49] Chain flexibility is set by a bond bending potential $U_{\mathrm{bend}} = k_\theta\ (1-\cos\theta)$, where θ is the angle between adjacent bonds and $k_\theta = 1.5\epsilon_{\mathrm{LJ}}$. Melts are prepared at constant volume and temperature with a monomer number density of $\rho = 0.85\sigma^{-3}$ and temperature of $k_BT = 1.0\epsilon_{\mathrm{LJ}}$. These conditions produce polymer melts with an entanglement segment length $N_e \approx 28$ beads,[50] an entanglement time $\tau_e \approx 1980\tau_{\mathrm{LJ}}$,[50−52] and a Rouse time $\tau_R^0 = \tau_e(N/N_e)^2 \approx 4041\tau_{\mathrm{LJ}}$.

Four bivalent associative groups (stickers) are evenly spaced along chain backbones by replacing regular monomers with associative "sticky" monomers. The stickers are placed on one of the two central monomers of each segment with length 10 monomers, producing an average sticker spacing of $N_s \approx 10$ beads. Bivalent stickers form stable dimers with cohesive energies U that are varied relative to k_BT to model dynamic networks with U/k_BT = 3, 6, 9, 12, 15, and 18. This captures the range of relative cohesive energies typical of hydrogen bonding networks.

Melts are simulated in LAMMPS and are equilibrated to a temperature $T = 1\epsilon_{\mathrm{LJ}}/k_B$ in the *NVT* ensemble within a periodic cubic box.[53] The equations of motion are integrated with a time step $\Delta t = 0.005\tau_{\mathrm{LJ}}$, and a Langevin thermostat maintains the temperature with a damping time $\tau_T = 100\tau_{\mathrm{LJ}}$. The center of mass velocity was periodically subtracted every 100 timesteps to remove center-of-mass drift due to Langevin forcing.

Tersoff Potential for Associative Bonds. Associative monomers interact with normal monomers through the LJ potential, but their interactions with each other are mediated by a Tersoff potential that forms reversible bivalent bonds. Once two associative monomers form a bond, a three-body energy penalizes other associative monomers from forming additional associative bonds with the bonded pair. We tune this three-body energy to control the preferred coordination of associative complexes and the kinetic barriers for the bond exchange process.

The Tersoff bond energy V_{ij} between two neighboring associative atoms is

$$V_{\mathrm{ij}} = f_C(r_{\mathrm{ij}})[f_R(r_{\mathrm{ij}}) + b_{\mathrm{ij}}f_A(r_{\mathrm{ij}})] \tag{1}$$

where f_R and f_A are, respectively, a repulsive and attractive pair potential, f_C is a smooth cutoff function, and b_{ij} is a bond order term that modifies the bond energy based on the coordination and geometry of neighboring atoms.[45]

The potentials f_R and f_A are the repulsive and attractive terms of a Morse potential

$$f_R(r) = Ae^{-\lambda_1 r} = Ue^{-2\alpha(r-r_0)} \tag{2}$$

$$f_A(r) = -Be^{-\lambda_2 r} = -2Ue^{-\alpha(r-r_0)} \tag{3}$$

where r_0 is the equilibrium bond length, U is the bond cohesive energy, and α is a curvature parameter that controls the width of the potential energy well (which implies $A = U$, $B = 2U$, $\lambda_1 = 2\alpha$ and $\lambda_2 = \alpha$).

The bond order b_{ij} is given by the function

$$b_{\mathrm{ij}} = (1 + \beta^n\zeta_{\mathrm{ij}}^n)^{-1/2n} \tag{4}$$

with numerical parameters β and n that set how rapidly the bond energy changes with increasing bond order. The function ζ_{ij} captures the species-specific contributions of neighboring atoms k to the bond order of the ij bond and is given by

$$\zeta_{\mathrm{ij}} = \sum_{\mathrm{k}\neq\mathrm{i,j}} f_C(r_{\mathrm{ik}})g(\theta_{\mathrm{ijk}})\exp[\lambda_3^m(r_{\mathrm{ij}} - r_{\mathrm{ik}})^m] \tag{5}$$

The contribution of atom k with a cutoff f_C on ζ_{ij} is based on the angular term $g(\theta_{\mathrm{ijk}})$ that accounts for the bond angle θ_{ijk} between bond ij and ik, and the exponential term $\exp[\lambda_3^m(r_{\mathrm{ij}} - r_{\mathrm{ik}})^m]$ that captures relative distances between bond ij and ik. In this paper, we have set $g(\theta_{\mathrm{ijk}}) = 1$ and the exponential term to 1 by making $\lambda_3 = 0$ and $m = 1$. This produces an isotropic potential for bivalent bonds that have no preferred orientation relative to the chain backbone.

An isotropic associative potential is consistent with choosing a coarse-grained scale for our bead−springs where each sticky bead does not represent one monomer but a larger segment of chain containing an associative group. In this limit, the associative potential of mean-force between two "sticky segments" can be isotropic, even if the underlying associative bonds are highly directional. Finer-scale details like directional bonding can be easily introduced by including the angular energy terms in the potential. These terms can capture a variety of open bonding geometries like dipolar hydrogen bonds and metal−ligand coordinations.

In the standard Tersoff model, f_C is a *universal* cutoff function for both V_{ij} and ζ_{ij}, defined as

$$f_C(r) = \begin{cases} 1, & r < R - D \\ \dfrac{1}{2} - \dfrac{1}{2}\sin\left(\dfrac{\pi}{2}\right), & R - D < r < R + D \\ 0, & r > R + D \end{cases} \tag{6}$$

which decreases from 1 to 0 over an interval $2D$ centered at the distance R.

V_{ij} and ζ_{ij} usually share the same cutoff function; however, we found this to be too restrictive when attempting to tune dimer and trimer cohesive energies and energy barriers, so we have defined two separate cutoff functions for V_{ij} and ζ_{ij}. Both functions use eq 6 but have distinct values for R and D that we refer to as (R_V, D_V) and (R_ζ, D_ζ) for V_{ij} and ζ_{ij}, respectively. We have added these modifications to the Tersoff potential in LAMMPS MD software, and the relevant source files are available through our group website.

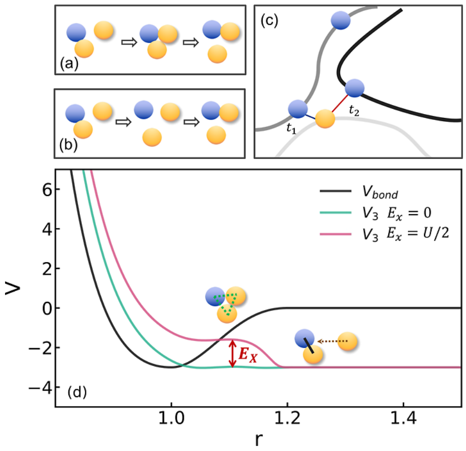

Figure 1. Schematic illustrations of (a) associative-type and (b) dissociative-type bond exchange processes, and (c) brachiation motion of a chain as it breaks a bond at time t_1 and forms a new one at time t_2 with a different chain segment. (d) Tersoff interaction potentials for two-body bond formation (V_{bond}, black) and three-body association (V_3). The three-body barrier is adjusted to vary the relative rate of associative-type and dissociative-type bond exchange processes.

The black curve in Figure 1d illustrates the two-body bond potential (V_{bond}) of a sticker pair as a function of their separation distance r when the sticky bond strength is $3k_BT$. Its shape is given by the Morse potential

$$V_{\mathrm{bond}} = f_R(r) + f_A(r) = Ue^{-2\alpha(r-r_0)} - 2Ue^{-\alpha(r-r_0)} \tag{7}$$

with an equilibrium bond distance $r_0 = 1.0\sigma$, well depth $U = 3k_BT$, and curvature parameter $\alpha = \sqrt{\kappa/2U} = 6\sigma^{-1}$ to control the width of the potential well, where κ sets the bond stiffness and vibration frequency.

The three-body energy V_3 for a third sticker to approach a bonded pair controls the coordination of associative clusters and the relative rates of many-body rearrangement processes. For dynamic networks with bivalent coordination, there are two commonly discussed rearrangement processes referred to as "associative-type" and "dissociative-type" bond exchange,[9,54,55] as illustrated in Figure 1a,b. Considering a lone sticker k and a sticky dimer pair ij, an associative-type exchange involves the formation of an intermediate trimer ijk that permits k to eject and replace i or j in the dimer. The second process is a dissociative-type bond exchange, where atom k waits for the ij dimer to dissociate into unpaired stickers through thermal activation and then takes one of them as a new partner. The relative activity of each process is controlled by the barrier E_x for trimer formation k + ij → ijk, as illustrated in Figure 1d. The Tersoff model can vary E_x over a wide range of values relative to U to simulate a variety of associative bond chemistries.

It is important to note that E_x cannot be made arbitrarily large independent of U. In fact, it cannot exceed the magnitude of the dimer cohesive energy U. This is because the most expensive barrier for sticker k to enter into a trimer with ij would be the case where k completely eliminates the ij bond. However, this also means that the jk and ik bonds would be destroyed in the trimer state, corresponding to a trimer energy of zero. Thus, the barrier magnitude is $E_x \le U$.

The barrier E_x can be set and manipulated in many ways, but we found that the simplest approach was to vary the cutoff range R and width D for the two different cutoff functions. Using brute-force parametric analysis, we determined the Tersoff parameters for the two models with different exchange barriers studied in this paper. The details of the parametrization process will be discussed in the following paragraphs. Parameters for both models are listed in Table 1. The parameters of model 1 produce a flat three-body potential surface, as shown in Figure 1d ($E_x = 0$). This flat landscape allows associative bond exchanges to occur whenever a third atom collides with a bonded pair. Under the same set of bond order parameters, shrinking the inner cutoff $r^{\zeta}_{\min} = (R_\zeta - D_\zeta)$ for ζ_{ij} allows us to create the three-body potential in Figure 1d ($E_x = U/2$) with an asymmetric barrier of $E_x = U/2$ for a trimer to form but almost no energy barrier for an atom to leave. This penalizes the formation of sticky trimers and makes them short-lived. The relative abundance of dissociative versus associative exchanges can be tuned by adjusting the height of the energy barrier.

Table 1. Tersoff Potential Parameters for the Two Models with Different Exchange Barriers E_x for Bivalent Bonding Studied in This Paper[a]

model	$E_x = 0$	$E_x = U/2$
R_ζ	$1 - 0.193877\frac{\sqrt{u}}{\sqrt{3}}$	$1 + 0.05\frac{\sqrt{u}}{\sqrt{3}}$
D_ζ	$0.393877\frac{\sqrt{u}}{\sqrt{3}}$	$0.15\frac{\sqrt{u}}{\sqrt{3}}$
β	31.449697	31.449697
n	1.451724	1.451724
R_V	$1 + 0.1\frac{\sqrt{u}}{\sqrt{3}}$	$1 + 0.1\frac{\sqrt{u}}{\sqrt{3}}$
D_V	$0.1\frac{\sqrt{u}}{\sqrt{3}}$	$0.1\frac{\sqrt{u}}{\sqrt{3}}$
α	$\frac{6\sqrt{3}}{\sqrt{u}}$	$\frac{6\sqrt{3}}{\sqrt{u}}$

[a] Parameters are adjusted relative to $u = U/k_BT$. These parameters can be divided into two parts: the first four define the shape of the three-body potential V_3; the last three define the shape of the pairwise potential V_{bond} between associative particles, which is the same for both exchange barriers.

Our Tersoff model parameters were selected through brute-force parametric analysis to optimize the shape of the three-body potential V_3. We first set the parameters of the two-body potential V_{bond} to be compatible with the bond lengths and vibrational time scales of the Kremer−Grest model. This is carried out by fixing the equilibrium distance of a sticky dimer pair $r_0 = 1.0\sigma$, the curvature parameter $\alpha = 6\sigma^{-1}$, and the cutoff distance $r^V_{\min} = (R_V - D_V) = 1.0\sigma$ and $r^V_{\max} = (R_V + D_V) = 1.2\sigma$ for V_{ij}. These parameters produce a two-body potential, as shown in Figure 1d. Once the two-body potential is set, the four remaining three-body parameters need to be defined: β, n, R_ζ, and D_ζ. We fix the outer cutoff distance $r^{\zeta}_{\max} = (R_\zeta + D_\zeta) = 1.2\sigma$ for ζ_{ij} to be consistent with $r^V_{\max}$ for V_{ij}. We treat the remaining bond order parameters β and n, and the inner cutoff distance $r^{\zeta}_{\min} = (R_\zeta - D_\zeta)$ for ζ_{ij} as optimization variables.

The optimization is performed by repeatedly evaluating the three-body potential V_3 of one associative monomer approaching a rigid associative dimer as β, n, and $r^{\zeta}_{\min}$ are systematically varied. Parameterizations are evaluated with a cost function that selects for specific shapes of the V_3 potential. We found that we could adequately describe the shape of V_3 by tracking the energy values associated with the local maxima, minima, and inflection points of the V_3 curve. To produce the flat V_3 function associated with $E_x = 0$, we defined our cost function to minimize the absolute difference between any energy minima, maxima, and inflection points relative to the cohesive energy U of the two-body potential. This identified the essentially flat potential plotted in Figure 1d for $U = 3k_BT$.

Extending our parametrizations to general values of U requires rescaling several model parameters. Increasing the cohesive energy U makes the two-body potential well deeper and bond vibrations faster, which could produce instabilities. To maintain a constant vibrational frequency, we fix the minimum of the two-body potential and rescale its width by adjusting the curvature parameter α and the outer cutoff distance $r^V_{\max} = (R_V + D_V)$ for V_{ij} by a factor $\propto\sqrt{u/3}$, where $u = U/k_BT$. This produces $\alpha = \frac{6}{\sqrt{(u/3)}}\sigma^{-1}$, $r^V_{\min} = 1.0\sigma$, and $r^V_{\max} = 1 + 0.2\frac{\sqrt{u}}{\sqrt{3}}\sigma$ for any values of cohesive energy U. To maintain the shape of V_3 relative to the two-body potential, we similarly rescale the three-body cutoff parameters $r^{\zeta}_{\min} = (R_\zeta - D_\zeta)$ and $r^{\zeta}_{\max} = (R_\zeta + D_\zeta)$. This produces the expressions reported in Table 1 that we have applied for all of the U studied.

Molecular Analysis. We measure the viscoelastic relaxation modulus $G(t)$ for reversible networks with the Green−Kubo method[56] by measuring the time correlations of the shear stress in equilibrium

$$G(t) = \frac{V}{k_BT}\langle\sigma_{\alpha\beta}(t)\cdot\sigma_{\alpha\beta}(0)\rangle \tag{8}$$

where V is the volume of the simulation box. We employ the multi-τ correlator algorithm[57] to compute the time correlation function and average over all three shear components of the stress tensor with $\alpha \neq \beta$.

Chain diffusion is measured by computing the mean-squared displacement (MSD) of individual monomers $g_1(t)$[49]

$$g_1(t) = \frac{1}{N_{\text{tot}}}\sum_{i=1}^{N_{\text{tot}}}\langle[\vec{r}_i(t) - \vec{r}_i(0)]^2\rangle \tag{9}$$

where $\vec{r}_i(t)$ is the position of a monomer at time t. The ensemble average is taken over all N_{tot} monomers including both sticky and nonsticky beads.

We identify associative bonds by measuring the separation between any two stickers and checking if they are within the inflection distance of the two-body binding energy, where $\partial^2V_{\text{bond}}/\partial r^2 = 0$. This corresponds to the peak restoring force of the bond, which decreases with further separation. We obtain a large set of bond histories in the form of Boolean-valued functions $s_i(t)$, where $s_i(t) = 1$ when bond i is

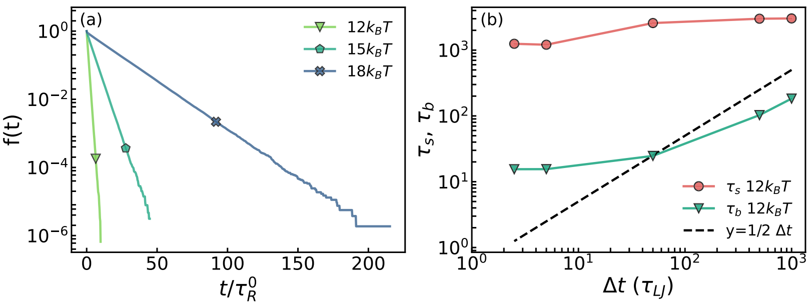

Figure 2. (a) Example of the correlation function of sticker lifetime τ_s for the zero barrier $E_x = 0$ system at $U/k_BT = 12$, 15, and 18. (b) Example of the measured τ_s and τ_b with varying chosen dumping time interval Δt. The black dashed line is the baseline for us to determine an appropriate Δt, where $y = \frac{1}{2}\Delta t$.

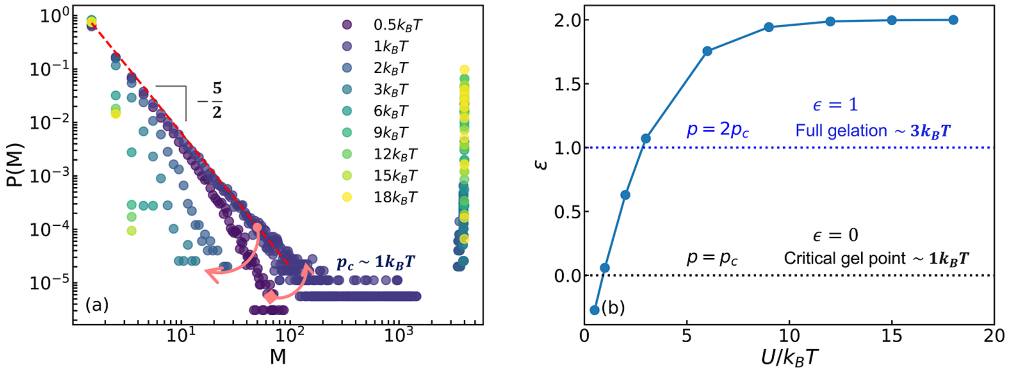

Figure 3. (a) Chain cluster size distribution with varying bond strengths. (b) Degree of gelation over increasing bond strengths according to the mean-field gelation theory.

formed and $s_i(t) = 0$ when it is broken. The bond lifetime is extracted by computing a bond lifetime correlation function

$$f(t) = \langle s(0)s(t)\rangle_i \tag{10}$$

averaged over all recorded lifetimes. As shown in Figure 2a for several systems, these lifetimes follow an exponential decay $f(t) = e^{-t/\tau_s}$ with a characteristic *sticky* bond lifetime τ_s.

The lifetime τ_s is a common descriptor for bond dynamics in associative networks, but it is not always the relevant time scale for network's viscoelasticity. In order to rearrange the macroscopic network, bonds must first break on a time scale τ_s^0, and then one of the lone stickers must make an excursion to find a partner in the network over a time scale τ_b. Following the work of Cai et al., we call this second lifetime of an unpaired sticker the "brachiation time".[58] In analogy to monkeys swinging through a canopy, the brachiation time τ_b measures the time required for a sticker on one chain to jump to a neighboring branch of the polymer network, as shown in Figure 1c. Similar to τ_s, the average brachiation time can also be obtained from the exponential slope of a correlation function for the *unpaired* lifetimes given by $(1 - s_i)$.

Measuring τ_s or τ_b with molecular simulations is nontrivial and sensitive to the time interval at which molecular configurations are sampled. Stickers attached to chain backbones move subdiffusively and frequently backtrack as they diffuse,[59] causing frequent recombination with old partners after breaking a bond. Each breaking event produces a bare bond lifetime τ_s^0 that is much faster than the network's stress relaxation because it is usually followed by a recombination. As the observation frequency is increased, the number of recorded recombination events tends to increase, and the measured value of τ_s tends to decrease. A more thorough analysis of this process is given in a recent study by Shanbhag and Ricarte.[59]

In this study, we measure a renormalized bond lifetime, τ_s, over which many recombination events occur until one of the original pairs finds a new partner and contributes to network relaxation. Note, τ_b is measured at high observation frequency, so we assume its value does not account for the recombination event of stickers. It is the time for stickers to stay alone or the traveling time for an unpaired sticker to form a pair after breakage with the previous one. The trajectory sampling frequency is calibrated by measuring the values of τ_s and τ_b for varying intervals from 2.5 to $1000\tau_{LJ}$ for each U/k_BT, as shown in Figure 2b. The measured values of τ_s and τ_b decrease with decreasing Δt until the interval is approximately half the measured relaxation time. Therefore, we limit our interval for recording system configurations to no more than half of the measured lifetime. In practice, this required some calibration runs until we could anticipate time scales for new systems through observed scaling relationships.

Each time a new associative bond is formed, we label it whether it is formed through an associative-type or dissociative-type bond exchange process. A bond formed at time frame t is considered to have formed through associative-type exchange if it had a different partner at time frame $t - 1$. Otherwise, we count it as a dissociative-type bond exchange process. We track the rates of active associative-type bond-swapping and passive dissociative-type dimerization per unpaired population of stickers as R_a and R_d, respectively. Since our time resolution is finite, this measure sets a lower bound on the rate of bond exchange since it is possible for associations to break or form in the time between our observations. However, the scaling of these rates appears to be robust for varying time intervals of analysis.

■ RESULTS AND DISCUSSION

As a first application of the reactive bead−spring model, we simulated the equilibrium self-assembly and viscoelasticity of dynamic polymer networks with binary associative complexes. By varying U/k_BT from 3 to 18, we observe a sol−gel transition and the development of network viscoelasticity consistent with experiments for associative polymers. We also perform a microscopic analysis of the associative bond kinetics for two model systems with different three-body energy barriers E_x. This permits us to test how macroscopic viscoelastic properties

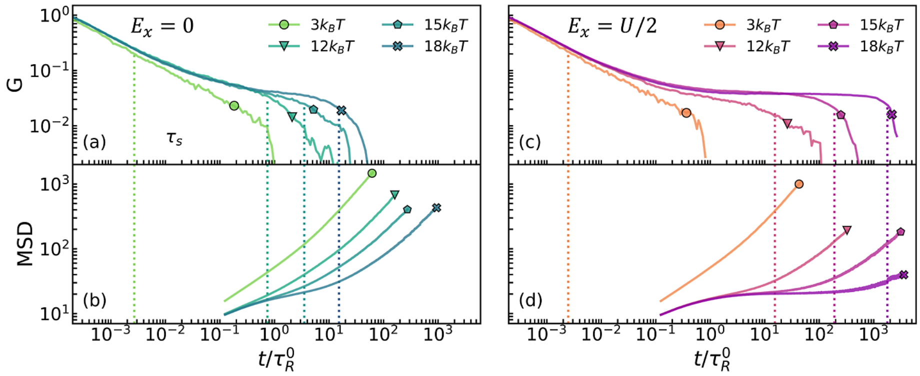

Figure 4. Network relaxation modulus of (a) systems with E_x = 0 and (c) systems with E_x = $U/2$ for varying sticky bond strengths in terms of simulation LJ time τ_{LJ} relative to original Rouse time τ_{R}^0. MSD of monomer over time with increasing sticky bond strengths for (b) systems with E_x = 0 and (d) systems with E_x = $U/2$. The vertical dotted lines indicate corresponding normalized sticker lifetime τ_s for different polymer systems with increasing $U/k_{\mathrm{B}}T$.

depend on associative bond kinetics with all other molecular features fixed.

Gel Point and Network Formation. The gel point and the sol−gel transition for the bead−spring dynamic networks are identified by measuring the equilibrium distribution $P(M)$ of chain clusters connected by associative bonds for varying $U/k_{\mathrm{B}}T$, as shown in Figure 3a. Here, M is the number of chains present in a bonded cluster, and $P(M)$ is the probability that any chain is part of a cluster of M bonded chains. For bond strengths below $1k_BT$, chains form only small clusters, but as U increases to $\sim 1k_BT$, a broad power-law distribution of chain cluster sizes develops, indicating a critical gel point p_c at $U/k_{\mathrm{B}}T \approx 1$ for this chain architecture and melt density. At the gel point, we observe a power-law cluster distribution $P(M) \sim M^{-5/2}$, consistent with the mean-field theory of gelation.[60] For higher $U/k_{\mathrm{B}}T$, a single peak at large M forms and grows as a percolating network cluster forms and incorporates an increasing number of chains into its structure.

The mean-field degree of gelation ϵ measures the proximity of the network topology to the critically percolated gel structure. It can be calculated from the equilibrium probability for a sticky monomer to be unpaired p_{open} as

$$\epsilon = \frac{p - p_c}{p_c} = \frac{(1 - p_{\mathrm{open}}) - p_c}{p_c} \tag{11}$$

where p is the probability of one sticky site being bonded, and $p_c = 1/(f - 1)$ is the critical bonding probability for gelation and is defined by the number of sticky sites per chain f. Figure 3b plots ϵ versus $U/k_{\mathrm{B}}T$ for our systems. As can be seen, $\epsilon = 0$ occurs just slightly below $U/k_{\mathrm{B}}T \sim 1$, consistent with the critical cluster size distribution that we observed for $P(M)$. As $U/k_{\mathrm{B}}T$ is increased above 1, ϵ increases to 1 by $U/k_{\mathrm{B}}T \approx 3$, indicative of a fully formed gel phase,[61,62] before saturating near $\epsilon = 2$. The saturation value corresponds to all stickers being paired ($p = 1$) and from plugging p_c in eq 11 is given by $\epsilon = f - 2$. This value depends on the number of associations per chain, which is $f = 4$ for our systems, thus limiting $\epsilon \leq 2$ no matter how large $U/k_{\mathrm{B}}T$ becomes.

Networks can form a variety of features, including dangling ends and self-loops, which impact the mechanical properties of the material. The simplest form of network defect is an intramolecular association in which two stickers on the same chain form a bond. Measuring the ratio of intramolecular to intermolecular associations provides a qualitative measure of the fraction of "defects" in the system. For all our systems, this fraction is ∼0.05 or less, independent of E_x (as expected). This small value is consistent with the short lengths of our chains and the high density of associative groups. Thus, we do not expect network defects to play a prominent role in the structure or behavior of the systems that we considered here.

Equilibrium Viscoelasticity and Chain Diffusion. Once past the gel point, the associative melts form transient networks that display a plateau in the linear viscoelastic relaxation modulus $G(t)$. Figure 4a,c shows simulated $G(t)$ for both models with E_x = 0 (left panels) and E_x = $U/2$ (right panels) for several values of $U/k_{\mathrm{B}}T$. Time on the x-axis is normalized by the Rouse relaxation time $\tau_{\mathrm{R}}^0 \approx 4041\tau_{\mathrm{LJ}}$ for the "unsticky" melt with no associative monomers. Values for τ_s measured from associative bond kinetics are indicated by the vertical dotted line. At short times, all systems display power-law stress relaxation consistent with the Rouse dynamics. This very early time regime is not affected by the presence of associations. For $U/k_{\mathrm{B}}T = 3$, the sticky relaxation time $\tau_s \ll \tau_{\mathrm{R}}^0$ and the associations do not alter the Rouse-like form of $G(t)$. This results in a network relaxation time $\tau_{\mathrm{N}} \approx \tau_{\mathrm{R}}^0$ for both the E_x = 0 and E_x = $U/2$ models. As $U/k_{\mathrm{B}}T$ increases, τ_s increases and becomes larger than τ_{R}^0, suppressing Rouse relaxation and producing a pronounced plateau in $G(t)$. The plateau extends to a terminal relaxation time, $\tau_{\mathrm{N}} \approx \tau_s$.

The plateau in stress relaxation directly corresponds to the delayed onset of chain diffusion. Figure 4b,d plots the monomer MSD $g_1(t)$ for chains in the same systems as panels (a and c). For both models with different E_x, a subdiffusive plateau in MSD develops and increases as τ_s increases above τ_{R}^0. The suppression of diffusion is stronger for the system with E_x = $U/2$ due to the suppression of associative-type bond-exchange kinetics with increasing $U/k_{\mathrm{B}}T$. For low $U/k_{\mathrm{B}}T$, the associations relax rapidly and produce excess dissipation, slightly altering the Rouse time but not altering the power-law form of the Rouse relaxation spectrum.

Our systems display terminal relaxation at $\tau_{\mathrm{N}} \approx \tau_s$ once $\tau_s > \tau_{\mathrm{R}}^0$. This is slightly different than the predictions of the sticky Rouse model, which predicts $\tau_{\mathrm{R}}^{\mathrm{s}} = \tau_s f^2$, where f is the number of stickers per chain. We attribute this difference to the small degree of gelation of our systems, which cannot be greater than $\epsilon = 2$ for our $f = 4$. In contrast, the predictions of the sticky Rouse model are made by assuming $f \gg 1$ and thus $\epsilon \gg 1$. When ϵ is large, chains must collectively dissociate many stickers in order to relax, producing sticky-Rouse scaling.

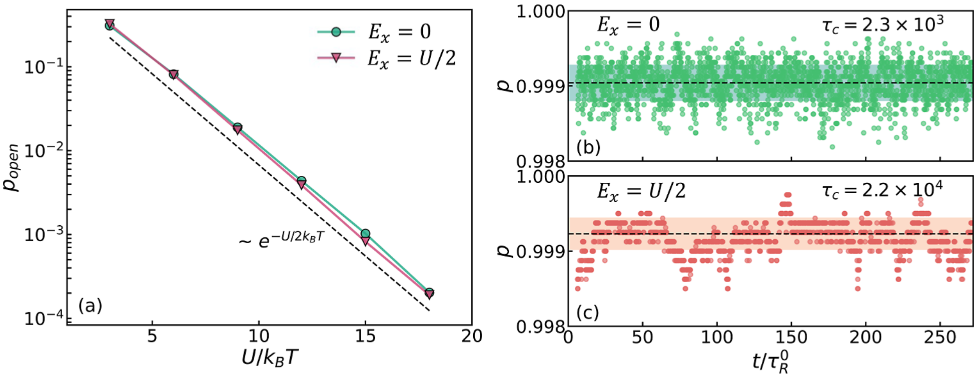

Figure 5. (a) Fraction of unpaired stickers p_{open} vs U/k_BT for the $E_x = 0$ and $E_x = U/2$ systems. The black dashed line indicates an exponential slope of −1/2. Equilibrium time evolution of chain connectivity ($p = 1 - p_{\text{open}}$) for (b) systems with $E_x = 0$ and (c) systems with $E_x = U/2$ at $U/k_BT = 15$. Time is normalized by the Rouse time of the unsticky melt $\tau_R{}^0 \approx 4041\tau_{LJ}$. A fluctuation relaxation time τ_c is measured for each system from the exponential decay of the time autocorrelation function of each series. The horizontal black dashed lines are the average values for each trajectory, and the highlighted regions indicate one standard deviation around the mean.

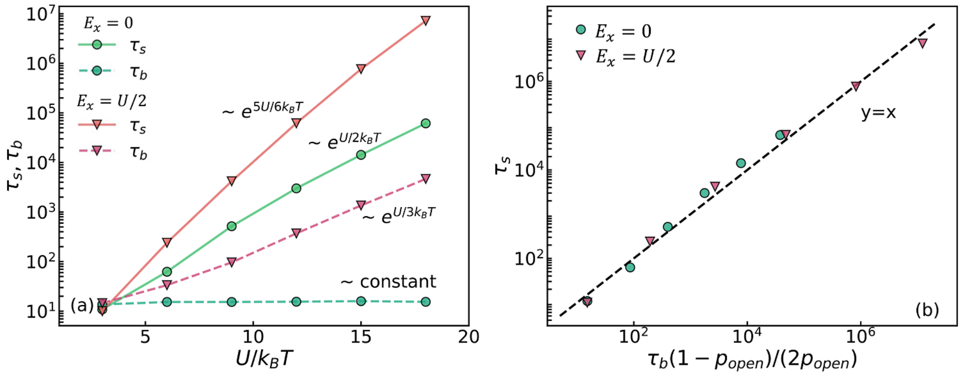

Figure 6. (a) Sticky bond lifetime τ_s and brachiation time of lone (unpaired) sticky monomers τ_b vs U/k_BT for systems with different exchange barriers $E_x = 0$ and $E_x = U/2$ in semilog scale with their corresponding slope fit. (b) Expression of sticker lifetimes τ_s as a function of brachiation time τ_b and the fraction of free stickers p_{open} for systems with different exchange barriers $E_x = 0$ and $E_x = U/2$. The dashed line is the function of $y = x$, which means that the values on the y-axis are equivalent to the values on the x-axis.

However, for systems that stay near the gel point with $\epsilon \sim 1$, chains need to dissociate only a few stickers to relax their conformations. This produces a terminal relaxation time of the same order as the sticky bond lifetime τ_s, as has been shown experimentally.[62,63]

The data in Figure 4 demonstrate the dramatic impact that the exchange barrier E_x has on gel transport and viscoelasticity. The suppression of trimer-mediated associative-type bond exchange makes gels much more sensitive to the temperature, resulting in much longer stress plateaus at the same value of U/k_BT. Since these differences are due to a kinetic barrier E_x and not the cohesive energy U of the associative complexes, the two systems display identical network plateau moduli G_N that are set by the maximum degree of gelation ($\epsilon = 2$) via the number of associations per chain. To understand how E_x impacts the temperature dependence of τ_s and τ_N, we next consider the detailed structure and kinetics of the associative bonds.

Equilibrium Network Structures and Fluctuations. In dynamic networks with binary complexes, sticky monomers can occupy one of two stable energy states: an open state with an association energy of $E_1 = 0k_BT$ and a closed state with an energy of $E_2 = -U/2$ per bonded particle in the binary complex. In thermal equilibrium, the probability that a sticky monomer is unbonded p_{open} will obey Boltzmann statistics

$$p_{\text{open}} = \frac{e^{-E_1/k_BT}}{e^{-E_1/k_BT} + e^{-E_2/k_BT}} \tag{12}$$

independent of the kinetics mediating associative bonding.[9] Figure 5a shows the fraction of unpaired stickers versus U/k_BT for both model networks with $E_x = 0$ (circles) and $E_x = U/2$ (triangles). Both models show the expected equilibrium structure, with p_{open} decreasing exponentially with U/k_BT with an exponential slope of −1/2.

While the kinetics of bond exchange does not influence the average number density of binary complexes, they do alter the time-correlations in the fluctuations around the average structure. The impact of E_x on fluctuations can be observed by plotting the fluctuations of network connections over time, as shown in Figure 5b,c. Both systems display similar averages and standard deviations, as expected from statistical mechanics, but the system with $E_x = 0$ fluctuates much more rapidly than the dissociative-type system with $E_x = U/2$. The correlation time scale of fluctuations for the $E_x = U/2$ system is 1 order of magnitude larger than that of the zero barrier $E_x = 0$ system for this $U/k_BT = 15$. This slowdown in network fluctuations is due to the exponential suppression of the rate of bond-swapping events due to the finite exchange barrier. These differences in equilibrium fluctuations are what give rise to the differences in viscoelasticity and chain mobility, as shown in Figure 4.

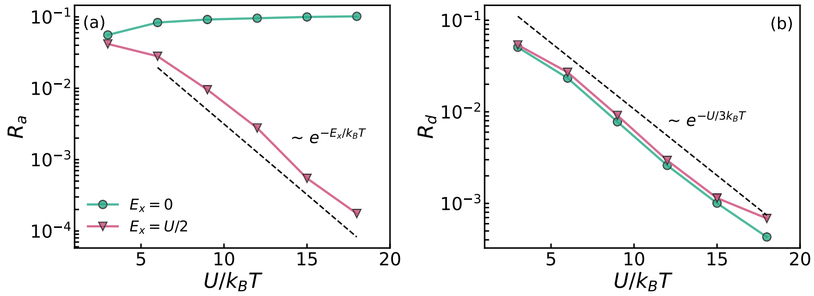

Figure 7. (a) Rate of associative-type bond exchange and (b) rate of dissociative-type exchange process per lone sticker per τ_{LJ} in terms of bond strengths U/k_BT for both models.

Molecular Kinetics of Associative Complexes. The kinetics of associative bond rearrangement can be characterized by several interrelated time scales, including the normalized sticky-bond lifetime τ_s and the sticker brachiation time τ_b. As discussed earlier, these time scales are subtly related. The lifetime τ_s captures the time required for sticky monomers to leave their current complex and form a new one with a new partner. The brachiation time τ_b measures the average time that sticky monomers spend alone, outside of any complex. These two time scales both contribute to the network relaxation time τ_N but display significantly different trends with the variation of the exchange barrier E_x/k_BT. Figure 6a plots τ_s and τ_b versus U/k_BT for both models. In both systems, τ_s increases exponentially with increasing U/k_BT, but at different rates. For $E_x = 0$, τ_s grows with an exponential slope of ∼1/2, while for $E_x = U/2$, τ_s grows more rapidly with an exponential slope ∼5/6.

Experimental studies have tried to relate exponential trends in τ_N or τ_s to the cohesive energies of the underlying associative bonds. Our results affirm that even when two systems have identical associative complexes and cohesive energies, the form of the exponential relationship between τ_s and U/k_BT is highly sensitive to the kinetics of higher-order bond rearrangement processes. Thus, when interpreting experimental data, it is important to both consider the cohesive energy of a complex U/k_BT, as well as the barriers for various bond exchange processes like E_x/k_BT.

The different scaling behaviors of τ_s with U/k_BT arise because exchange barrier E_x extends the time that lone stickers require to form new complexes. This delay is measured by the "brachiation" times τ_b, plotted as dashed lines in Figure 6a. For the model with $E_x = 0$, τ_b is constant, showing no change with increasing U/k_BT. This is because there is no barrier to associative-type bond exchange, so lone stickers can always easily find new partners by forming a trimer with an existing associative complex. In contrast, τ_b for the $E_x = U/2$ system shows an exponential increase with U/k_BT with an exponential prefactor of ∼1/3. This is due to E_x exponentially suppressing the associative-type exchange process as U/k_BT increases.

Since new associations can only form when lone stickers form new complexes, either with another monomer or through associative-type exchange with an existing dimer, we expect $\tau_s \sim \tau_b$. Thus, the different trends in τ_s versus U/k_BT for the two models are fully captured by the different scalings for the brachiation time τ_b. To see why this is so, consider that the total number of sticky monomers can be partitioned into two populations, $N_s = N_m + N_d$, with N_m unpaired stickers monomers and N_d stickers paired into $N_d/2$ dimers. Each of the N_m unpaired stickers will form new complexes over a time $\sim \tau_b$. This will refresh the fraction $N_m/(N_d/2)$ of the network connections. We expect the associative bond relaxation rate to be $\tau_s^{-1} = 2\tau_b^{-1}N_m/N_d$. Given that $N_m = N_s p_{open}$ and $N_d = N_s(1 - p_{open})$, we obtain a relationship

$$\tau_s = \frac{\tau_b}{2}\frac{(1 - p_{open})}{p_{open}} \sim \tau_b e^{U/2k_BT} \qquad (13)$$

The relation of eq 13 is plotted in Figure 6b and works well for all simulated systems at all values of U/k_BT and E_x/k_BT. Equation 13 shows that trends in τ_s with U/k_BT can be broken into two contributions. The exponential term $e^{U/2k_BT}$ does not depend on model kinetics and occurs because associative bond rearrangement is driven by the population of unpaired stickers which is exponentially suppressed, as shown in Figure 5a. Thus, the only way in which the kinetics of associative bond exchange can impact τ_s is through changes in the brachiation time τ_b for unpaired stickers.

We can relate changes in τ_b to the relative rates of the specific bond exchange processes. Figure 7a,b plots rates for associative-type R_a and dissociative-type R_d bond exchange events, respectively, for all values of U/k_BT and E_x/k_BT. As expected, the associative-type exchange rate R_a is exponentially suppressed by the exchange barrier E_x, scaling as $R_a \sim e^{-E_x/k_BT}$. This results in a rapid suppression of the associative-type exchange process for systems with $E_x = U/2$ but little change in the rate for systems with $E_x = 0$. In constrast, R_d displays similar scaling $\sim e^{-U/3k_BT}$ for all systems, independent of E_x. This is because dissociative-type exchanges are mediated by unpaired stickers forming bonds with each other, and the fraction p_{open} only depends on U/k_BT in equilibrium (Figure 5a).

For $E_x = 0$ and large U/k_BT, bond rearrangements are dominated by associative-type exchanges with $R_a/R_d \sim 10^3$ at the largest U/k_BT we consider. This is approaching the behavior of vitrimer-like covalent adaptive networks. Since there is no barrier to trimer formation, lone stickers are annihilated whenever they encounter a dimer, which will depend on the density and arrangement of stickers on chain backbones rather than the bond strength. For the $E_x = U/2$ systems, R_a is suppressed faster than R_d with $R_a/R_d \sim 10^{-1}$ at the highest $U/k_BT = 18$, producing systems dominated by dissociative-type exchange events, similar to hydrogen bonding networks. These trends illustrate how the character of bond exchange kinetics in coordinated associative networks depends on both U/k_BT and E_x/k_BT and will generally involve both types of processes as the temperature is varied.

Note, in this study, we have varied U/k_BT by varying the cohesive energy U at fixed k_BT. In practice, experiments are more likely to vary the temperature k_BT, which will also alter the rate of monomer diffusion since diffusion coefficients $D \sim k_BT$. If sticker recombination is diffusion limited, then τ_s and τ_b can display additional temperature dependence $\sim D^{-1} \sim T^{-1}$. While this is a much weaker effect than the exponential scaling observed in Figure 6, it could be significant when U/k_BT is small.

CONCLUSIONS

We have presented a new reactive coarse-grained model for simulating associative polymers with precisely coordinated associative complexes. Our model adds a many-body Tersoff potential to the standard Kremer-Grest bead−spring model to capture the precise coordination and kinetics of associative complex formation at coarse-grained scales. This allows us to use efficient bead−spring simulations to study the structure and processing of associative polymers mediated by a wide variety of dynamic bonding mechanisms and relate the macroscopic viscoelasticity of networks to the microscopic kinetics of their associative bonds. This study demonstrated two models for dynamic networks with binary associative complexes, reminiscent of hydrogen bonding polymer networks. However, the Tersoff potential can be easily extended to more complex associative interactions.

Our simple model has just two adjustable parameters, a cohesive energy U/k_BT for binary complexes, and an energy barrier E_x/k_BT for bond exchange. By varying E_x/k_BT, we can tune the associative-type/dissociative-type character of the network kinetics at a fixed network structure. We verified self-assembly behavior by identifying a gelation transition at $U/k_BT \approx 1$ and comparing it to the Flory−Stockmayer theory. The resulting networks developed stress plateaus with terminal relaxation times $\tau_N \sim \tau_s$, consistent with experiments.[62,63] By examining the associative bond kinetics, we found a simple scaling relationship relating the lifetime τ_s of associative complexes to the brachiation time τ_b that quantifies how long lone stickers spend unpaired $\tau_s \sim \tau_b e^{U/2k_BT}$. This relationship reveals that the exchange barrier E_x/k_BT only influences τ_s through the brachiation time τ_b.

Using a many-body potential energy instead of probabilistic Monte Carlo moves to model associative bonding enables us to apply our model *predictively* rather than *prescriptively* to study nonequilibrium systems. The rates of associative bond formation and dissociation emerge naturally from the energy landscape of the reactive potential and thus do not need to be prescribed beforehand as is required for Monte Carlo. This allows us to predict how associative bond kinetics vary with changes in association placement along chain backbones and chain architecture. Furthermore, the reactive hamiltonian and its dynamics remains valid in nonequilibrium conditions. Studies of the impact of associative interactions on chain dynamics during nonlinear flow are the subject of our forthcoming research.

We expect that these models will be a valuable tool for understanding the dynamics of associative polymer processing and processability. While associative networks are gaining popularity as nominally recyclable and reprocessable plastic materials, in many cases, we still do not know how to reliably process these materials to begin with. We hope that this model will provide a new and efficient approach for tackling these challenges and enabling the adoption of more sustainable and recyclable plastics.

AUTHOR INFORMATION

Corresponding Author

Thomas C. O'Connor − *Department of Materials Science and Engineering, Carnegie Mellon University, Pittsburgh, Pennsylvania 15213, United States;* orcid.org/0000-0002-9393-0295; Email: thomaso@andrew.cmu.edu

Author

Songyue Liu − *Department of Materials Science and Engineering, Carnegie Mellon University, Pittsburgh, Pennsylvania 15213, United States*

Complete contact information is available at: https://pubs.acs.org/10.1021/acs.macromol.3c02022

Notes

The authors declare no competing financial interest.

ACKNOWLEDGMENTS

The authors acknowledge startup funding support through Carnegie Mellon University's Department of Materials Science and Engineering, and support from the Office of Naval Research NEPTUNE program through grant number N000142312635. Part of this research was conducted using the Tartan Research Advanced Computing Environment (TRACE), a shared computational resource provided by the College of Engineering at Carnegie Mellon University.

REFERENCES

(1) Webber, M. J.; Tibbitt, M. W. Dynamic and reconfigurable materials from reversible network interactions. *Nat. Rev. Mater.* **2022**, *7*, 541−556.

(2) Mendes, A. C.; Baran, E. T.; Reis, R. L.; Azevedo, H. S. Self-assembly in nature: Using the principles of nature to create complex nanobiomaterials. *Wiley Interdiscip. Rev.: Nanomed. Nanobiotechnol.* **2013**, *5*, 582−612.

(3) Schroeder, L. R.; Cooper, S. L. Hydrogen bonding in polyamides. *J. Appl. Phys.* **1976**, *47*, 4310−4317.

(4) Garcia, D.; Starkweather, H. W. HYDROGEN BONDING IN NYLON 66 AND MODEL COMPOUNDS. *J. Polym. Sci., Polym. Phys. Ed.* **1985**, *23*, 537−555.

(5) Chowdhury, S. C.; Gillespie, J. W. A molecular dynamics study of the effects of hydrogen bonds on mechanical properties of Kevlar® crystal. *Comput. Mater. Sci.* **2018**, *148*, 286−300.

(6) Wemyss, A. M.; Ellingford, C.; Morishita, Y.; Bowen, C.; Wan, C. Dynamic Polymer Networks: A New Avenue towards Sustainable and Advanced Soft Machines. *Angew. Chem., Int. Ed.* **2021**, *60*, 13725−13736.

(7) Cordier, P.; Tournilhac, F.; Soulié-Ziakovic, C.; Leibler, L. Self-healing and thermoreversible rubber from supramolecular assembly. *Nature* **2008**, *451*, 977−980.

(8) Kloxin, C. J.; Bowman, C. N. Covalent adaptable networks: Smart, reconfigurable and responsive network systems. *Chem. Soc. Rev.* **2013**, *42*, 7161−7173.

(9) Wu, S.; Chen, Q. Advances and New Opportunities in the Rheology of Physically and Chemically Reversible Polymers. *Macromolecules* **2022**, *55*, 697−714.

(10) Semenov, A. N.; Rubinstein, M. Thermoreversible Gelation in Solutions of Associative Polymers. 1. Statics. *Macromolecules* **1998**, *31*, 1373−1385.

(11) Rubinstein, M.; Semenov, A. N. Thermoreversible Gelation in Solutions of Associating Polymers. 2. Linear Dynamics. *Macromolecules* **1998**, *31*, 1386−1397.

(12) Baxandall, L. G. Dynamics of Reversibly Cross-Linked Chains. *Macromolecules* **1989**, *22*, 1982−1988.

(13) Leibler, L.; Rubinstein, M.; Colby, R. H. Dynamics of Reversible Networks. *Macromolecules* **1991**, *24*, 4701−4707.

(14) Rubinstein, M.; Semenov, A. N. Dynamics of entangled solutions of associating polymers. *Macromolecules* **2001**, *34*, 1058−1068.

(15) Lodge, A. S.; Armstrong, R. C.; Wagner, M. H.; Winter, H. H. Constitutive Equations from Gaussian Molecular Network Theories in Polymer Rheology. *Pure Appl. Chem.* **1982**, *54*, 1349−1359.

(16) Mohottalalage, S. S.; Senanayake, M.; Clemmer, J. T.; Perahia, D.; Grest, G. S.; O'Connor, T. Nonlinear Elongation Flows in Associating Polymer Melts: From Homogeneous to Heterogeneous Flow. *Phys. Rev. X* **2022**, *12*, 021024.

(17) Hoy, R. S.; Fredrickson, G. H. Thermoreversible associating polymer networks. I. Interplay of thermodynamics, chemical kinetics, and polymer physics. *J. Chem. Phys.* **2009**, *131*, 131.

(18) Wilson, M.; Rabinovitch, A.; Baljon, A. R. Computational Study of the Structure and Rheological Properties of Self-Associating Polymer Networks. *Macromolecules* **2015**, *48*, 6313−6320.

(19) Amin, D.; Likhtman, A. E.; Wang, Z. Dynamics in supramolecular polymer networks formed by associating telechelic chains. *Macromolecules* **2016**, *49*, 7510−7524.

(20) Perego, A.; Khabaz, F. Volumetric and Rheological Properties of Vitrimers: A Hybrid Molecular Dynamics and Monte Carlo Simulation Study. *Macromolecules* **2020**, *53*, 8406−8416.

(21) Amin, D.; Wang, Z. Nonlinear rheology and dynamics of supramolecular polymer networks formed by associative telechelic chains under shear and extensional flows. *J. Rheol.* **2020**, *64*, 581−600.

(22) Kumar, S. K.; Douglas, J. F. Gelation in physically associating polymer solutions. *Phys. Rev. Lett.* **2001**, *87*, 188301.

(23) Wang, S.; Chen, C. C.; Dormidontova, E. E. Reversible association and network formation in 3:1 ligand-metal polymer solutions. *Soft Matter* **2008**, *4*, 2039−2053.

(24) Oyarzún, B.; Mognetti, B. M. Efficient sampling of reversible cross-linking polymers: Self-assembly of single-chain polymeric nanoparticles. *J. Chem. Phys.* **2018**, *148*, 114110.

(25) Sciortino, F. Three-body potential for simulating bond swaps in molecular dynamics. *Eur. Phys. J. E* **2017**, *40*, 3.

(26) Rovigatti, L.; Nava, G.; Bellini, T.; Sciortino, F. Self-Dynamics and Collective Swap-Driven Dynamics in a Particle Model for Vitrimers. *Macromolecules* **2018**, *51*, 1232−1241.

(27) Ciarella, S.; Sciortino, F.; Ellenbroek, W. G. Dynamics of Vitrimers: Defects as a Highway to Stress Relaxation. *Phys. Rev. Lett.* **2018**, *121*, 058003.

(28) Ciarella, S.; Biezemans, R. A.; Janssen, L. M. C. Understanding, predicting, and tuning the fragility of vitrimeric polymers. *Proc. Natl. Acad. Sci.* **2019**, *116*, 25013−25022.

(29) Ciarella, S.; Ellenbroek, W. G. Associative bond swaps in molecular dynamics. *SciPost Physics* **2022**, *12*, 128.

(30) Ciarella, S.; Ellenbroek, W. G. Swap-driven self-adhesion and healing of vitrimers. *Coatings* **2019**, *9*, 114.

(31) Paciolla, M.; Likos, C. N.; Moreno, A. J. Validity of Effective Potentials in Crowded Solutions of Linear and Ring Polymers with Reversible Bonds. *Macromolecules* **2022**, *55*, 2659−2674.

(32) Kulshreshtha, A.; Hayward, R. C.; Jayaraman, A. Impact of Composition and Placement of Hydrogen-Bonding Groups along Polymer Chains on Blend Phase Behavior: Coarse-Grained Molecular Dynamics Simulation Study. *Macromolecules* **2022**, *55*, 2675−2690.

(33) Jiang, N.; Zhang, H.; Yang, Y.; Tang, P. Molecular dynamics simulation of associative polymers: Understanding linear viscoelasticity from the sticky Rouse model. *J. Rheol.* **2021**, *65*, 527−547.

(34) Roh, E. J.; Baig, C. Nonequilibrium Monte Carlo simulations of entangled polymer melts under steady shear flow. *Soft Matter* **2019**, *15*, 5271−5281.

(35) Jayaraman, A. 100th Anniversary of Macromolecular Science Viewpoint: Modeling and Simulation of Macromolecules with Hydrogen Bonds: Challenges, Successes, and Opportunities. *ACS Macro Lett.* **2020**, *9*, 656−665.

(36) Bertrand, C. E.; Liu, Y. Molecular dynamics of a model dimerizing fluid. *J. Chem. Phys.* **2015**, *142*, 044503.

(37) Ghobadi, A. F.; Jayaraman, A. Effect of backbone chemistry on hybridization thermodynamics of oligonucleic acids: A coarse-grained molecular dynamics simulation study. *Soft Matter* **2016**, *12*, 2276−2287.

(38) Ghobadi, A. F.; Jayaraman, A. Effects of Polymer Conjugation on Hybridization Thermodynamics of Oligonucleic Acids. *J. Phys. Chem. B* **2016**, *120*, 9788−9799.

(39) Condon, J. E.; Jayaraman, A. Development of a Coarse-Grained Model of Collagen-Like Peptide (CLP) for Studies of CLP Triple Helix Melting. *J. Phys. Chem. B* **2018**, *122*, 1929−1939.

(40) Farah, K.; Müller-Plathe, F.; Böhm, M. C. Classical reactive molecular dynamics implementations: State of the art. *ChemPhysChem* **2012**, *13*, 1127−1151.

(41) Liang, T.; Shin, Y. K.; Cheng, Y. T.; Yilmaz, D. E.; Vishnu, K. G.; Verners, O.; Zou, C.; Phillpot, S. R.; Sinnott, S. B.; Van Duin, A. C. Reactive potentials for advanced atomistic simulations. *Annu. Rev. Mater. Res.* **2013**, *43*, 109−129.

(42) O'Connor, T. C.; Andzelm, J.; Robbins, M. O. AIREBO-M: A reactive model for hydrocarbons at extreme pressures. *J. Chem. Phys.* **2015**, *142*, 024903.

(43) Liang, T.; Shan, T. R.; Cheng, Y. T.; Devine, B. D.; Noordhoek, M.; Li, Y.; Lu, Z.; Phillpot, S. R.; Sinnott, S. B. Classical atomistic simulations of surfaces and heterogeneous interfaces with the charge-optimized many body (COMB) potentials. *Mater. Sci. Eng., R* **2013**, *74*, 255−279.

(44) Chenoweth, K.; Van Duin, A. C.; Goddard, W. A. ReaxFF reactive force field for molecular dynamics simulations of hydrocarbon oxidation. *J. Phys. Chem. A* **2008**, *112*, 1040−1053.

(45) Tersoff, J. New empirical approach for the structure and energy of covalent systems. *Phys. Rev. B* **1988**, *37*, 6991−7000.

(46) Marrink, S. J.; Tieleman, D. P. Perspective on the martini model. *Chem. Soc. Rev.* **2013**, *42*, 6801−6822.

(47) Yesylevskyy, S. O.; Schäfer, L. V.; Sengupta, D.; Marrink, S. J. Polarizable water model for the coarse-grained MARTINI force field. *PLoS Comput. Biol.* **2010**, *6*, 1−17.

(48) Marrink, S. J.; Risselada, H. J.; Yefimov, S.; Tieleman, D. P.; De Vries, A. H. The MARTINI force field: Coarse grained model for biomolecular simulations. *J. Phys. Chem. B* **2007**, *111*, 7812−7824.

(49) Kremer, K.; Grest, G. S. Dynamics of entangled linear polymer melts: A molecular-dynamics simulation. *J. Chem. Phys.* **1990**, *92*, 5057−5086.

(50) Moreira, L. A.; Zhang, G.; Müller, F.; Stuehn, T.; Kremer, K. Direct equilibration and characterization of polymer melts for computer simulations. *Macromol. Theory Simul.* **2015**, *24*, 419−431.

(51) Hsu, H. P.; Kremer, K. Static and dynamic properties of large polymer melts in equilibrium. *J. Chem. Phys.* **2016**, *144*, 144.

(52) Ge, T.; Robbins, M. O.; Perahia, D.; Grest, G. S. Healing of polymer interfaces: Interfacial dynamics, entanglements, and strength. *Phys. Rev. E: Stat., Nonlinear, Soft Matter Phys.* **2014**, *90*, 012602.

(53) Plimpton, S. Fast Parallel Algorithms for Short-Range Molecular Dynamics. *J. Comput. Phys.* **1995**, *117*, 1−19.

(54) Scheutz, G. M.; Lessard, J. J.; Sims, M. B.; Sumerlin, B. S. Adaptable Crosslinks in Polymeric Materials: Resolving the Intersection of Thermoplastics and Thermosets. *J. Am. Chem. Soc.* **2019**, *141*, 16181−16196.

(55) Van Zee, N. J.; Nicolaÿ, R. Vitrimers: Permanently crosslinked polymers with dynamic network topology. *Prog. Polym. Sci.* **2020**, *104*, 101233.

(56) Kubo, R.; Toda, M.; Hashitsume, N. *Statistical Physics II: Nonequilibrium Statistical Mechanics*; Springer: Berlin, 1985.

(57) Likhtman, A. E.; Sukumaran, S. K.; Ramirez, J. Linear viscoelasticity from molecular dynamics simulation of entangled polymers. *Macromolecules* **2007**, *40*, 6748−6757.

(58) Cai, P. C.; Krajina, B. A.; Spakowitz, A. J. Brachiation of a polymer chain in the presence of a dynamic network. *Phys. Rev. E* **2020**, *102*, 020501.

(59) Shanbhag, S.; Ricarte, R. G. On the Effective Lifetime of Reversible Bonds in Transient Networks. *Macromol. Theory Simul.* **2023**, *32*, 2300002.
(60) Rubinstein, M.; Colby, R. H. *Polymer Physics*; Oxford University Press, 2003.
(61) Li, D. T.; Rudnicki, P. E.; Qin, J. Distribution Cutoff for Clusters near the Gel Point. *ACS Polymers Au* **2022**, *2*, 361−370.
(62) Zhang, Z.; Chen, Q.; Colby, R. H. Dynamics of associative polymers. *Soft Matter* **2018**, *14*, 2961−2977.
(63) Chen, Q.; Huang, C.; Weiss, R. A.; Colby, R. H. Viscoelasticity of reversible gelation for ionomers. *Macromolecules* **2015**, *48*, 1221−1230.

https://doi.org/10.1021/acs.macromol.3c02022
Macromolecules 2024, 57, 1403−1413